Original Article

JSA

J Strain Analysis
1–7

DOI: 10.1177/0309324717723274
journals.sagepub.com/home/sdj
SAGE

Evaluation of Hertzian contact parameters from whole field displacement data

M.P Hariprasad and K. Ramesh

Abstract

Evaluation of contact parameters in Hertzian contact from displacement data is studied. Based on complex potential approach, generic explicit equations for displacement field in the vicinity of the contact zones are presented. Methodology for evaluating unknown contact parameters and associated rigid body displacements from the whole field experimental displacement data is implemented using an over-deterministic system of equations in a least squares sense. Usefulness of this method in dealing different contacting geometries is brought out by analyzing different contacting situations using digital image correlation.

Keywords

Contact mechanics, explicit displacement equations, digital image correlation, Muskhelishvili complex potential, rigid body displacement

Date received: 4 May 2017; accepted: 30 June 2017

Introduction

Contact zones present in the interface of any systems are crucial as such regions serve in load transfer from one component to another. Knowledge of the contact parameters between the contacts is necessary to optimize the design of components in such regions. Analytical modeling of stress fields by complex potential approach in the vicinity of the contact zones is available in the literature.[1–5] However, the explicit displacement equations available in the literature are only for the contact interface or along a line of symmetry.[1,2] In 2003, Kourkoulis et al.[6] have reported an explicit equation for the displacement fields based on complex potential approach for contacting situation of a disc jaw assembly having different predetermined radius of curvature.

Digital photoelasticity[7] has been effectively applied in obtaining the contact stress parameters from the whole field principal stress difference data.[7–10] Digital image correlation (DIC) is a whole field optical non-destructive experimental technique to obtain the displacement/strain fields which is gaining prominence in many engineering applications.[11–13] However, attempts to utilize the whole field displacement data for contact zone analysis are limited in the literature.[6,14] The main issue with the displacement data is the non-uniqueness of the displacement field due to rigid body motion.[2,3] In this article, the displacement field near contact zone for Hertzian contact is presented. Then, a methodology is proposed to evaluate the contact length and rigid body motions associated with the displacement data from the experimentally obtained whole field displacements using a nonlinear least squares method.

Whole field displacement near contact zone

Schematic diagram of the contact zone is shown in Figure 1. The interface between the contact zones is assumed to be perfectly smooth and hence, the loading is assumed to be normal to the contacting interface. The problem is modeled as a two-dimensional (2D) plane stress elasticity problem where Muskhelishvili's[3] complex potentials approach is used to simulate the Hertzian contact field. Complex potential used in

Department of Applied Mechanics, Indian Institute of Technology Madras, Chennai, India

Corresponding author:
K. Ramesh, Department of Applied Mechanics, Indian Institute of Technology Madras, Chennai 600036, India.
Email: kramesh@iitm.ac.in

Kourkoulis et al.[6] is particular to a specific contacting radii, which is given as $\Phi(z) = 1/6RA(\sqrt{(a^2 - z^2)} + iz)$.

Following the study of Kourkoulis et al.,[6] in this work a generic displacement equation is proposed by incorporating the relative radius of curvature term (η) in the Muskhelishvili's potential (Φ) which is given as

$$\Phi(z) = \frac{\eta}{2A}\left(\sqrt{(a^2 - z^2)} + iz\right) \tag{1}$$

Here, η refers to the relative curvature between the contacting surface, which is given as

$$\eta = \left(\frac{1}{R_1} + \frac{1}{R_2}\right)$$

Here, R_1 and R_2 are the radius of curvature of the two contacting bodies. In equation (1), a is semi-contact length (Figure 1), and z is a complex number defined as $z = x + iy$. For similar bodies, A is defined as $A = (k + 1)/(2G)$ where G is the shear modulus, and k is the Kolosov's constant. It is defined as $k = (3 - \nu)/(1 + \nu)$ and $k = (3 - 4\nu)$ for plane stress and plane strain situations, respectively, with ν as Poisson's ratio.

The potential function given in equation (1) can be used for different contacting situations. The relative curvature η takes a value of $2/R$ when both the contacting bodies have same radius R and $\eta = (1/R)$ if one of the surfaces has an infinite radius (flat). Furthermore, it can be seen that on setting $R_2 = -1.5R_1$, equation (1) gives $\Phi(z) = 1/6RA(\sqrt{(a^2 - z^2)} + iz)$ which is same as given in Kourkoulis et al.[6]

From the Muskhelishvili's potential (Φ), whole field strains and displacement data can be expressed as[2–4]

$$2G\left[\frac{\partial u}{\partial x} + i\frac{\partial u}{\partial y}\right] = (z - \bar{z})\bar{\Phi}'(\bar{z}) + \Phi(\bar{z}) + k\Phi(z) \tag{2}$$

$$2G[u + iv] = k\varphi(z) + \varphi(\bar{z}) + (\bar{z} - z)\overline{\varphi'(\bar{z})} + T \tag{3}$$

In equations (2) and (3), prime denotes the derivative and bar represents the complex conjugate. The term T represents the rigid body motion associated with the displacement data.[3] Here, $\varphi(z)$ is obtained by integrating the Muskhelishvili's potential (Φ) once. The displacement is obtained by substituting equation (1) into equation (3) and by separating the real and imaginary parts of equation (3), the horizontal (u) and vertical (v) components of the displacement can be expressed as

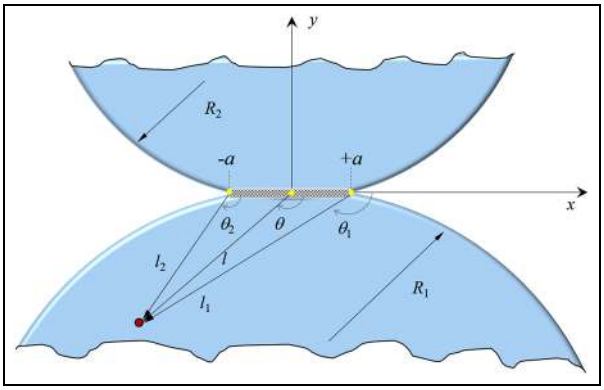

Figure 1. Schematic diagram of the contact zone of two discs in contact.

$$\begin{aligned}
&2Gu(l,\theta) = \frac{\eta}{4A}\Big\{(k-1)\Big[l^2\sin2\theta - l(l_1l_2)^{\frac{1}{2}}\sin(\theta + (\theta_1 + \theta_2)/2) + \\
&0.5a^2\left[\arctan\frac{l\sin\theta + (l_1l_2)^{\frac{1}{2}}\sin((\theta_1 + \theta_2)/2)}{l\cos\theta + (l_1l_2)^{\frac{1}{2}}\cos((\theta_1 + \theta_2)/2)} - \arctan\frac{l\sin\theta - (r_1r_2)^{\frac{1}{2}}\sin((\theta_1 + \theta_2)/2)}{l\cos\theta - (l_1l_2)^{\frac{1}{2}}\cos((\theta_1 + \theta_2)/2)}\right]\Big] \\
&+ 4l\sin\theta\Big[l\cos\theta - (l_1l_2)^{\frac{1}{2}}\cos((\theta_1 + \theta_2)/2)\Big]\Big\} - \chi\times l\sin\theta + T_x
\end{aligned} \tag{4}$$

$$\begin{aligned}
&2Gv(l,\theta) = \\
&\frac{\eta}{4A}\Big\{(k+1)\Big[l^2\cos2\theta - l(l_1l_2)^{\frac{1}{2}}\cos(\theta + (\theta_1 + \theta_2)/2) \\
&+ \frac{a^2}{4}\ln\frac{l^2 + l_1l_2 + 2l(l_1l_2)^{\frac{1}{2}}\cos(\theta - (\theta_1 + \theta_2)/2)}{l^2 + l_1l_2 - 2l(l_1l_2)^{\frac{1}{2}}\cos(\theta - (\theta_1 + \theta_2)/2)}\Big] \\
&+ 4l\sin\theta\Big[l\sin\theta - (l_1l_2)^{\frac{1}{2}}\sin((\theta_1 + \theta_2)/2)\Big]\Big\} \\
&+ \chi\times l\cos\theta + T_y
\end{aligned} \tag{5}$$

With the definitions

$$l_{2,1} = \sqrt{l^2 \pm a^2 - 2la\cos\theta} \text{ and } \theta_{2,1} = \arctan\frac{l\sin\theta}{l\cos\theta \pm a}$$

In equations (4) and (5), χ represents the rigid body rotation term, and T_x and T_y are the rigid body translation terms along x- and y-directions, respectively. Radial (u_r) and tangential (u_θ) components of the displacement fields from u and v are obtained as

$$u_r = u\cos\theta + v\sin\theta \tag{6}$$

$$u_\theta = -u\sin\theta + v\cos\theta \tag{7}$$

Substituting equations (4) and (5) into equation (6), one can see that the radial component of the displacement (u_r) is not affected by the rigid body rotation term (χ) as the rotation components get canceled. This makes it (u_r) the right choice of data to be processed for further analysis.

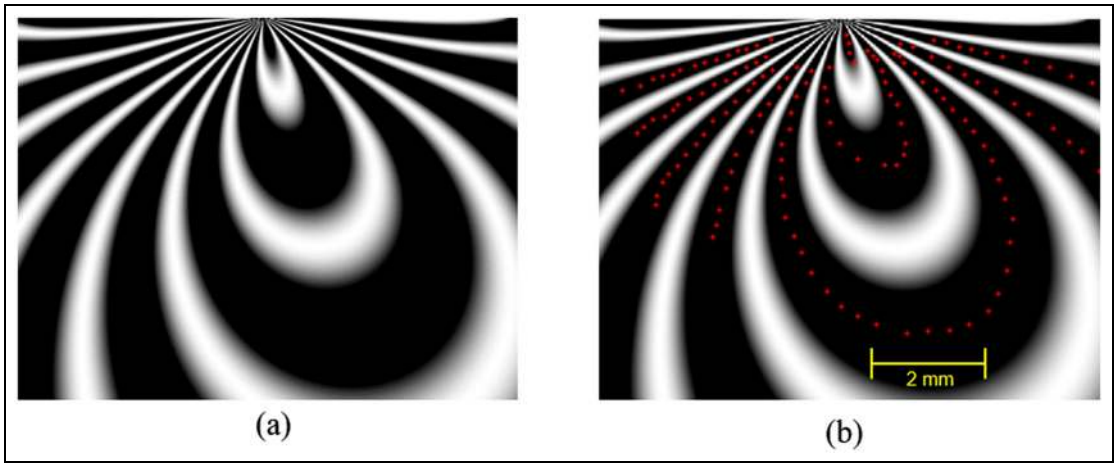

Figure 2. Pseudo fringes of radial displacement ($M = 40$) from (a) analytical data for $a = 3$, $T_x = 0.1$, $T_y = -0.5$ and (b) reconstructed using the parameters obtained from the nonlinear least squares method with data points echoed back.

Contact parameter evaluation from displacement data using nonlinear least squares

In this section, a methodology to extract the unknown contact length and rigid body translation from the whole field displacement data is established. Combining equation (6) and the experimental radial displacement data, following the study of Ramesh et al.,[15] an error function is defined for the n^{th} data point in the model domain as

$$g_n = u_r(a, T_x, T_y) - u_r^{\exp} \tag{8}$$

As the error function g_n is nonlinear in terms of a, this needs an iterative procedure of least squares analysis by minimizing the error function. This is done based on the Taylor series expansion of the error function, and it can be expressed in terms of g_n and correction factor of the parameters $(\Delta a, \Delta T_x, \Delta T_y)$ for i^{th} iteration as

$$-(g_n)_i = \left(\frac{\partial g_n}{\partial a}\right)_i (\Delta a)_i + \left(\frac{\partial g_n}{\partial T_x}\right)_i (\Delta T_x)_i + \left(\frac{\partial g_n}{\partial T_y}\right)_i (\Delta T_y)_i \tag{9}$$

Application of equation (9) to n data points can be represented in matrix form as

$$\begin{Bmatrix} g_1 \\ g_2 \\ \vdots \\ g_n \end{Bmatrix}_i = - \begin{bmatrix} \frac{\partial g_1}{\partial a} & \frac{\partial g_1}{\partial T_x} & \frac{\partial g_1}{\partial T_y} \\ \frac{\partial g_2}{\partial a} & \frac{\partial g_2}{\partial T_x} & \frac{\partial g_2}{\partial T_y} \\ \vdots & \vdots & \vdots \\ \frac{\partial g_n}{\partial a} & \frac{\partial g_n}{\partial T_x} & \frac{\partial g_n}{\partial T_y} \end{bmatrix}_i \begin{Bmatrix} \Delta a \\ \Delta T_x \\ \Delta T_y \end{Bmatrix}_i \tag{10}$$

This set of equations are solved in an over-deterministic approach, and the parameters are then modified in the $i + 1$ iteration based on the correction terms $\Delta a, \Delta T_x$ and ΔT_y obtained.

Initially, this methodology is verified for its correctness with analytically generated displacement data with known values of a, T_x and T_y using equations (4) and (5). In order to process the displacement data, one has to collect the positional coordinates and corresponding displacements from the contact field. In photoelastic data analysis, it has been established that collecting data on fringe contours gives improved results for crack as well as contact stress parameters.[16] Following this, the displacement data are represented as pseudo-Moiré contours using the expression $255\cos(u_r \times M)$, where M is used to control the density of the pseudo-Moiré fringes. Value of M is selected such that there are sufficient number of fringes for data collection. Displacement field with $a = 3$ mm, $T_x = 0.1$ mm and $T_y = -0.5$ mm is analytically generated and is shown as pseudo fringe contours ($M = 40$) in Figure 2(a). The displacement data and corresponding positional coordinates are collected from the vicinity of the contact field and are then processed in a least squares sense. The values obtained are same as that of the one used for analytical generation. The contact zone is then reconstructed (Figure 2(b)) with the results obtained from least squares analysis and the data used for the analysis are echoed back on the reconstructed image. The results obtained from the least squares analysis are in agreement with the given simulated parameters, and this indicates the correctness of the implemented procedure.

Experimental analysis

Experimental setup

The 2D DIC experiments are performed at the interface of two discs under compressive load. Discs of 60-mm diameter ($\eta = 2/R$) are made with epoxy material having Young's modulus of $E = 3300$ MPa and Poisson's ratio of $\nu = 0.37$. A loading fixture is designed and fabricated for obtaining a normal load between the two discs. The models are speckled initially by spraying a matt white paint followed by matt black paint

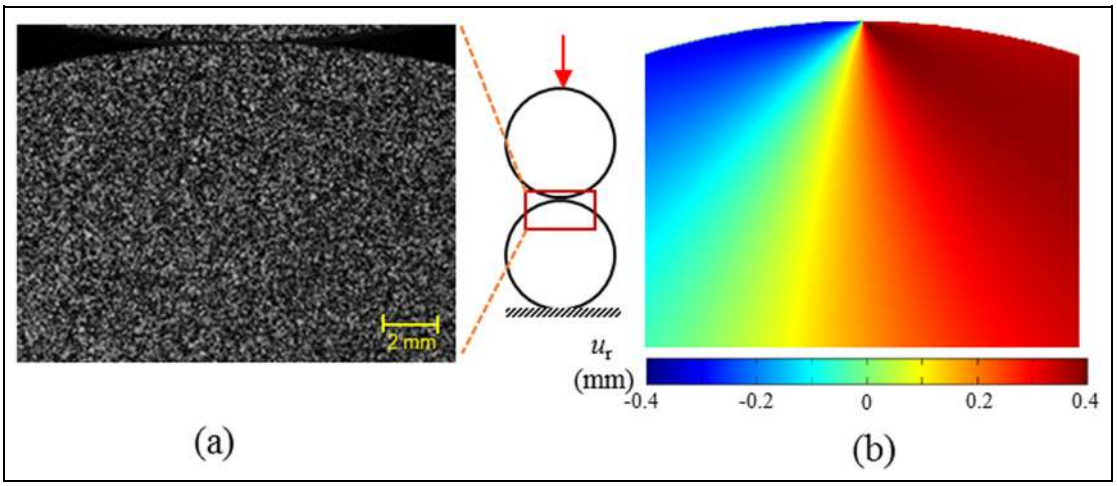

Figure 3. (a) Speckled model for reference image and (b) contour plot of the u_r displacement obtained from DIC analysis.

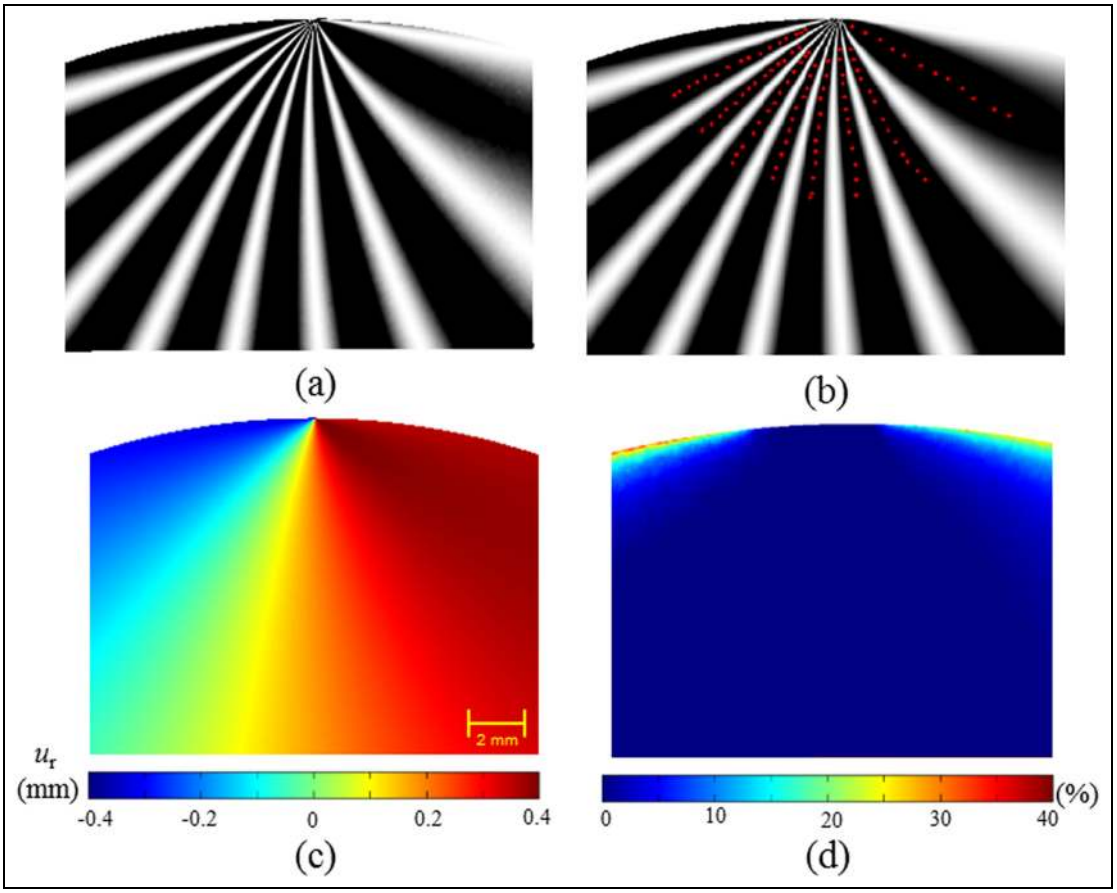

Figure 4. Pseudo fringes of radial displacement from (a) experimental results from DIC, (b) reconstructed using the parameters obtained from the nonlinear least squares method with data points echoed back, (c) contour plot of the u_r displacement shown in (b) and (d) error plot of u_r displacement.

randomly over the model. Contact zone of the disc assembly before the loading, which is used as the reference image, is shown in Figure 3(a). The magnification of the speckled image is 84 pixel/mm, and about 73% of the speckles are found to have size less than 4 pixels. A load of 600 N is applied on the top disc using a universal tensile testing machine with a loading rate of 5 N/s and the images are captured using GRAS-20S4M-C camera (1624×1224 pixels and 8-bit dynamic range) with a Tokina 100-mm f/2.8 lens with light-emitting diode (LED) illumination. Deformed speckle images are then analyzed using a commercial package

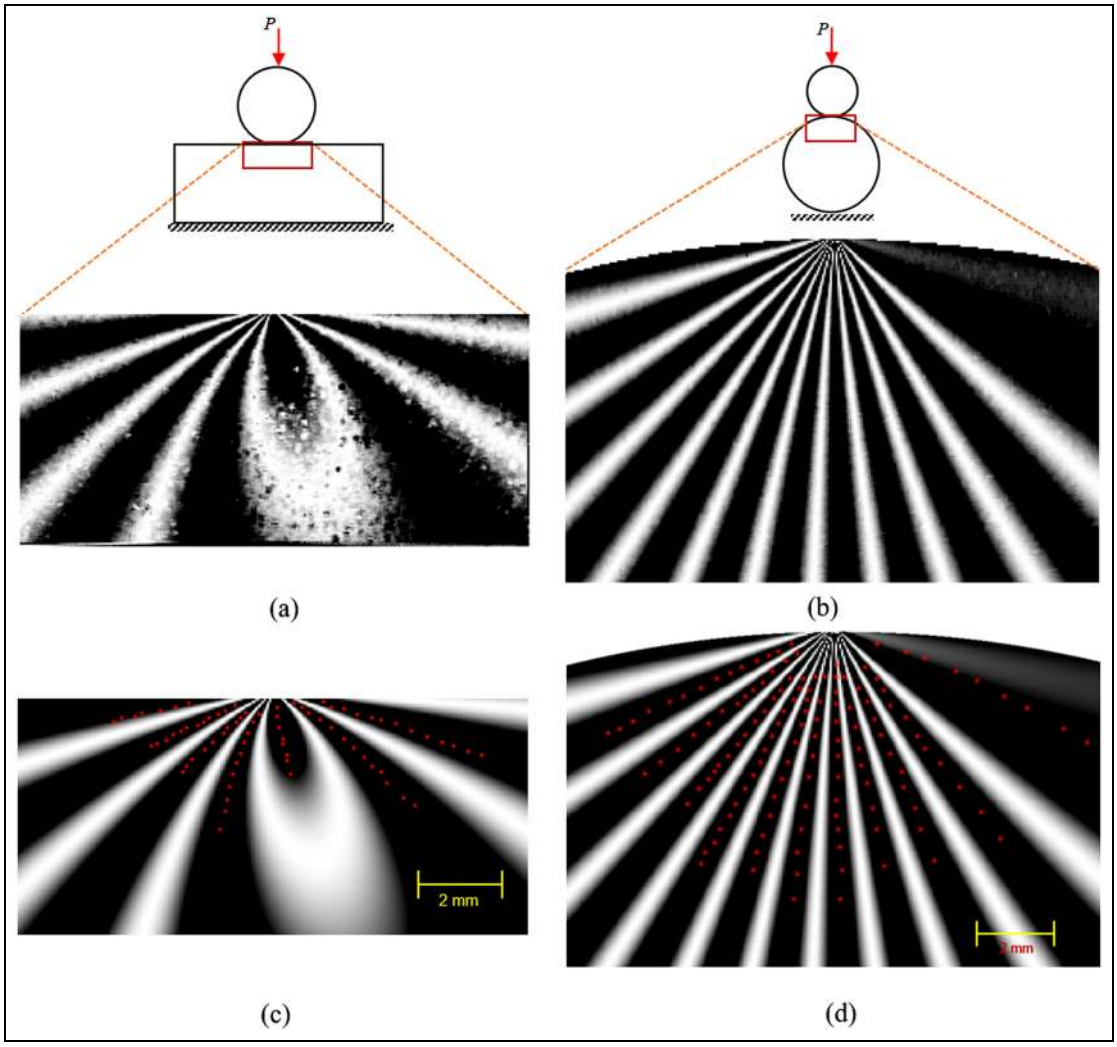

Figure 5. Pseudo fringes of radial displacement from experimental DIC results for (a) $\eta = 1.85/R$, (b) $\eta = 2.85/R$. Reconstructed using the parameters obtained from the nonlinear least squares method with data points echoed back for contact zone with (c) $\eta = 1.85/R$ and (d) $\eta = 2.85/R$.

VIC-2D to obtain the displacement fields in the vicinity of the contact zone. The selection of DIC parameters are problem specific, and here, these are selected (subset size of 21 pixels with a step size of 5) such that there is minimum loss in the data near the contact interfaces with good correlation in the entire field. Here, only the lower disc is considered, and the whole field experimental radial displacement (u_r) obtained from the DIC result is shown as a contour plot in Figure 3(b).

Contact parameter evaluation from experimental displacement data

Displacement data obtained from DIC result is post-processed to obtain the contact parameters using nonlinear least squares algorithm. Figure 4(a) shows the pseudo fringe contours ($M = 70$) of experimental radial displacement. From the analysis, the semi-contact length a is obtained as 1.1 mm, and the rigid body translations T_x and T_y are obtained as 0.34 and -0.24 mm, respectively.

Figure 4(b) shows the reconstructed pseudo fringe contour along with the data points echoed back on the reconstructed radial displacement data obtained from the analysis. Displacement variation is shown as a colored contour plot in Figure 4(c). Whole field error in the displacement obtained between the experimental and least squares modeling is shown in Figure 4(d). It is clear from Figure 4(d) that the estimated contact parameters from the experimental data are able to model the contact zone accurately. Unlike in the study of Kourkoulis et al.,[6] where a correction of the displacement is required, here, the rigid body terms are also evaluated as part of the analysis.

As one could see that the displacement equations (equations (4) and (5)) reported in this study are not limited to the contact zones having same radius of curvature. To illustrate this, two different cases having different radii of curvatures for contact interface is

Table 1. Results obtained for different contacting interfaces.

R_1	R_2	η	Semi-contact length, a (mm)	Rigid body translation—x-direction, T_x (mm)	Rigid body translation—y-direction, T_y (mm)
R	R	$2/R$	1.1	0.34	−0.24
Infinite radius	$0.542R$	$1.85/R$	1.09	0.036	−0.17
R	$0.542R$	$2.85/R$	0.79	1.18	−0.33

$R = 30$ mm; T_x, T_y, R_1 and R_2 are in mm.

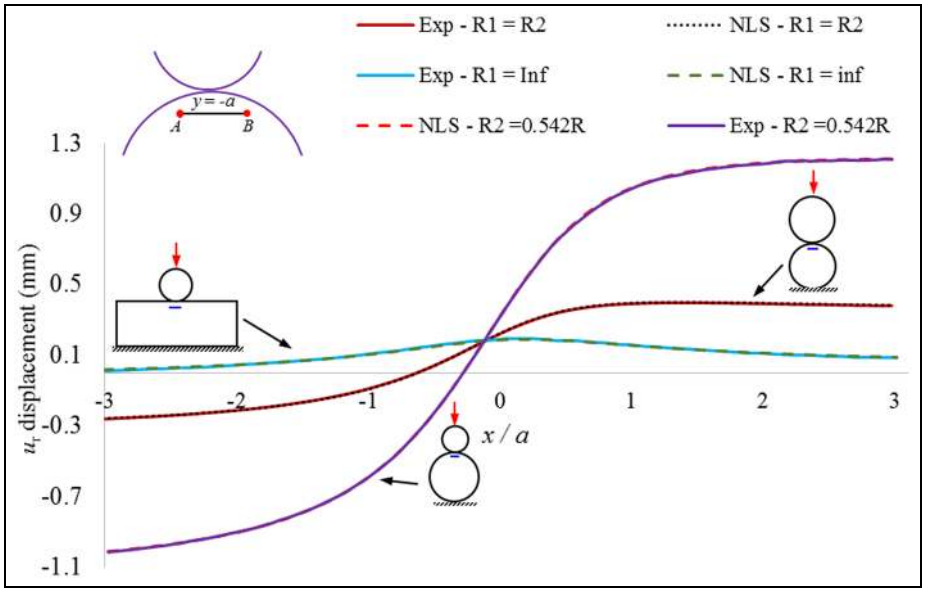

Figure 6. Variation of the radial displacement along x/a at $y = -a$ for experimental and least squares model for three cases of contacting situations.

considered next. Figure 5(a) and (b) show the experimental pseudo fringe contours obtained using subset and step sizes of 17 and 5 with $M = 35$ for $\eta = (1.85/R)$ and $\eta = (2.85/R)$, respectively, where $R = 30$ mm. The magnification is of 106 pixel/mm, and 64% of the speckles are of size less than 4 pixels. These data are then processed as described in previous sections, and the reconstructed contours generated from the parameters obtained with data echoed back are shown in Figure 5(c) and (d). Results obtained from the experimental displacement data for various problems are consolidated in Table 1.

Variation of the radial displacement estimated from the least squares method compared with experimental results from DIC along x/a at $y = -a$ for various contact zones are shown in Figure 6. An error analysis conducted on the robustness of the nonlinear least squares algorithm revealed that the displacement data should have an accuracy better than 0.001 mm to estimate contact parameters within an error of 0.5%. In VIC-2D, the displacements can have resolution up to 0.00001 times the field of view (FOV). In this study, the FOV was in the range of 15–19 mm, and the data can be measured with a maximum resolution of 0.00015 mm. In the case of contact zone measurements, the speckles should have a good contrast and variation in the intensity with lower speckle sizes even at higher magnifications. In view of the strain gradients in contact zones, the choice of subset size cannot be of higher values as it may over smooth the actual displacement data and also loose data at the boundaries. These factors are problem dependent, and one has to exercise special care in selecting these parameters appropriately for a given experimental situation.

Closure

Displacement field for contact zones involving nonconformal geometries are presented in a generic sense. Evaluation of contact zone using the whole field experimental displacement data, where the contact parameters are unknown is implemented. The displacement data obtained from DIC is post-processed to obtain the contact length along with the rigid body components of the displacement field. Three different cases of contact zones are evaluated, and the proposed method is verified for its usefulness in dealing with a variety of contacting situations by appropriately changing the relative curvature term η. Since DIC can be done on actual

components, this methodology will be very useful in real-life industrial applications.

Declaration of conflicting interests

The author(s) declared no potential conflicts of interest with respect to the research, authorship and/or publication of this article.

Funding

The author(s) received no financial support for the research, authorship and/or publication of this article.

References

1. Johnson KL. *Contact mechanics*. Cambridge: Cambridge University Press, 2003.
2. Hills DA, Nowell D and Sackfield A. *Mechanics of elastic contacts*. Oxford: Butterworth Heinemann Ltd., 1993.
3. Muskhelishvili NL. *Some basic problems of the mathematical theory of elasticity*. 4th ed. Berlin: Springer, 1977.
4. Sackfield A, Mugadu A and Hills DA. The influence of an edge radius on the local stress field at the edge of a complete fretting contact. *Int J Solids Struct* 2002; 39: 4407–4420.
5. Smith JO and Liu CK. Stresses due to tangential and normal loads on an elastic solid with application to some contact stress problems. *J Appl Mech* 1953; 20: 157–166.
6. Kourkoulis SK, Markides CF and Chatzistergos PE. The standardized Brazilian disc test as a contact problem. *Int J Rock Mech Min* 2013; 57: 132–141.
7. Ramesh K. *Digital photoelasticity: advanced techniques and applications*. Berlin, Heidelberg: Springer, 2000.
8. Sukla A and Nigam HA. Numerical–experimental analysis of the contact stress problem. *J Strain Anal Eng Des* 1985; 20(4): 241–245.
9. Frankovský P, Ostertag O, Trebuňa F, et al. Methodology of contact stress analysis of gearwheel by means of experimental photoelasticity. *Appl Opt* 2016; 55(18): 4856–4864.
10. Hariprasad MP and Ramesh K. Contact zone evaluation of dental implants using digital photoelasticity. In: Korach CS, Tekalur SA and Zavattieri P (eds) *Mechanics of biological systems and materials: proceedings of the society for experimental mechanics series*, vol. 6. Berlin: Springer, 2016, pp.39–43.
11. Dixie MH, James CG and Andrew WD. Experimental methodology using digital image correlation to assess ballistic helmet blunt trauma. *J Appl Mech* 2011; 78(5): 051022.
12. McCormick NJ and Lord JD. Practical in situ applications of DIC for large structures. *Appl Mech Mater* 2010; 24–25: 161–166.
13. Du Y, Diaz EA, Burgete RL, et al. Evaluation of DIC of stress intensity factor in an aerospace panel. *Experiment Mech* 2011; 51: 45–57.
14. Kourkoulis SK, Markides CF and Chatzistergos PE. The Brazilian disc under parabolically varying load. *Int J Solids Struct* 2012; 49: 959–972.
15. Ramesh K, Gupta S and Kelkar AA. Evaluation of stress field parameters in fracture mechanics by photoelasticity: revisited. *Eng Fract Mech* 1997; 9: 189–210.
16. Ramesh K, Ramesh B and Vivekanandan A. Evaluation of interaction effects in multiple cracks under biaxial loads using photoelasticity. In: *Proceedings of the Society of Engineering Science 52nd annual technical meeting*, College Station, TX, 26–28 October 2015.